

# Approximating Ground States of Quantum Hamiltonians with Snapshot-QAOA

Reuben Tate<sup>\*¶</sup>, Quinn Langfitt<sup>§</sup>, Elijah Pelofske<sup>†</sup>, Ammar Kirmani<sup>‡</sup>,  
Andreas Bärtzsch<sup>\*</sup>, John Golden<sup>\*</sup> and Stephan Eidenbenz<sup>\*</sup>

<sup>\*</sup>CCS-3: Information Sciences, Los Alamos National Laboratory, Los Alamos, NM, U.S.A.

<sup>†</sup>A-1: Information Systems and Modeling, Los Alamos National Laboratory, Los Alamos, NM, U.S.A.

<sup>‡</sup>T-4: Physics of Condensed Matter and Complex Systems, Los Alamos National Laboratory, Los Alamos, NM, U.S.A.

<sup>§</sup>Computer Science Department, Northwestern University, Evanston, IL, U.S.A.

<sup>¶</sup>Corresponding Author Email: rtate@lanl.gov

**Abstract**—We present Snapshot-QAOA, a variation of the Quantum Approximate Optimization Algorithm (QAOA) that finds approximate minimum energy eigenstates of a large set of quantum Hamiltonians (i.e. Hamiltonians with non-diagonal terms). Traditionally, QAOA targets the task of approximately solving combinatorial optimization problems — Snapshot-QAOA enables a significant expansion of the use case space for QAOA to more general quantum Hamiltonians, where the goal is to approximate the ground-state. Such ground-state finding is a common challenge in quantum chemistry and material science applications. Snapshot-QAOA retains desirable variational-algorithm qualities of QAOA, in particular small parameter count and relatively shallow circuit depth. Snapshot-QAOA is thus a better trainable alternative to the NISQ-era Variational Quantum Eigensolver (VQE) algorithm, while retaining a significant circuit-depth advantage over the QEC-era Quantum Phase Estimation (QPE) algorithm. Our fundamental approach is inspired by the idea of Trotterization of a continuous-time linear adiabatic anneal schedule, which for sufficiently large QAOA depth gives very good performance. Snapshot-QAOA restricts the QAOA evolution to not phasing out the mixing Hamiltonian completely at the end of the evolution, instead evolving only a partial typical linear QAOA schedule, thus creating a type of snapshot of the typical QAOA evolution. As a test case, we simulate Snapshot-QAOA on a particular 16 qubit  $J_1$ - $J_2$  frustrated square transverse field Ising model with periodic boundary conditions.

## I. INTRODUCTION

The Quantum Approximate Optimization Algorithm (QAOA) [1, 2], which was also generalized under the same acronym to the Quantum Alternating Operator Ansatz [3], was introduced as a near-term quantum hardware-friendly algorithm that could, given sufficient parameter training and circuit depth, sample optimal or good approximate solutions of combinatorial optimization problems.

Typically, QAOA is studied as a quantum algorithm that is intended to sample solutions, ideally optimal or nearly optimal solutions, of classical discrete combinatorial optimizations problems (i.e. the decision variables are binary, or spins). A considerable amount of study has been applied to this form of QAOA, including potential evidence for speedups over other quantum algorithms or existing classical optimization solvers [4–7] as well as generalizations of QAOA to include, for

example, more complex mixing Hamiltonians and different initial states [3, 8–12].

In this work we propose Snapshot-QAOA, which allows a significant expansion of the typical capabilities of QAOA to include a broad class of quantum Hamiltonians (meaning Hamiltonians with non-diagonal terms). The fundamental computational ideas used in this study are based on adiabatic quantum computation and transverse field driven quantum annealing in particular [13–16].

Snapshot-QAOA is well-suited for Hamiltonians of the form  $c_0 H_0 + c_1 H_1$ , i.e. a linear combination of two sub-Hamiltonians  $H_0$  and  $H_1$ , where the ground state of  $H_0$  is non-degenerate and easy to prepare, and where the corresponding unitaries  $e^{-i\alpha H_0}$  and  $e^{-i\alpha H_1}$  are easily implementable on a quantum computer for any  $\alpha \in \mathbb{R}$ . The key insight is that, for such Hamiltonians  $H$ , for any  $T > 0$ , there exists a linear annealing schedule with an associated time-dependent Hamiltonian  $\mathcal{H}_T(t)$  for which the “snapshot” of  $\mathcal{H}(t)$  at some time  $t = \tau$  is exactly  $H$ , i.e.,  $H = \mathcal{H}_T(\tau)$ . We show that this relationship allows one to easily determine suitable  $T$ -dependent values of the usual QAOA circuit parameters (typically denoted by  $\vec{\gamma}$  and  $\vec{\beta}$ ), thus causing Snapshot-QAOA to converge towards the ground state energy as the number of QAOA layers,  $p$ , increases. Thus, Snapshot-QAOA only has one parameter ( $T$ ) that requires tuning. This last property means that one does not necessarily need to perform variational learning on the usual QAOA circuit parameters ( $\vec{\gamma}$  and  $\vec{\beta}$ ) in order to achieve good performance; however, we do show like with standard QAOA, optimizing  $\vec{\gamma}$  and  $\vec{\beta}$  further based on the schedules given by Snapshot-QAOA can indeed yield improved performance over the Trotterized non-optimized schedule.

The above Snapshot-QAOA properties are significant because while there do exist relatively short-depth quantum algorithm approaches to approximate the ground-states of quantum Hamiltonians, namely variational quantum algorithms such as the Variational Quantum Eigensolver (VQE) [17, 18], typically these algorithms contain a large number of trainable parameters which makes the black-box optimizer machine learning loop quite difficult in general, especially for standard

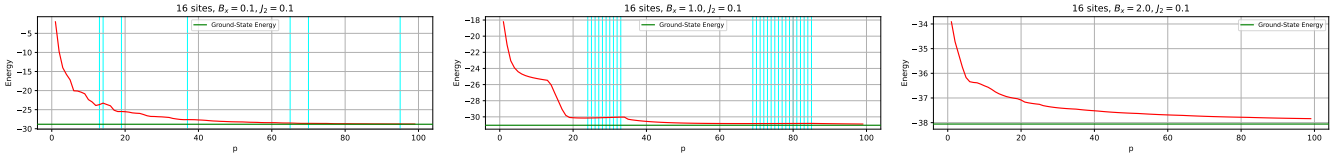


Fig. 1. Convergence plots of Snapshot-QAOA, with energy (y-axis) as a function of  $p$  (x-axis). Known ground-state energy, computed using exact diagonalization  $\mathcal{E}_H$  is shown by the horizontal green line. The optimized  $T$  parameter was found by a linearly spaced gridsearch between  $[0, p]$  in steps of 0.01, meaning that many of these  $T$  parameters could potentially be improved with better optimization, in particular for values greater than  $p$  or higher precision searches within  $[0, p]$ . If any energy value for a particular  $p + 1$  is higher energy than  $p$ , meaning the simulation decreased in quality, that  $p$  index is marked by a vertical cyan line.

black-box optimizers. In the other extreme, Quantum Phase Estimation (QPE) is a quantum algorithm that is used as subroutine for finding ground-states of quantum Hamiltonians, but requires extremely large circuits to implement and is therefore typically considered in the realm of only being feasible with full-scale Quantum Error Correction (QEC) [19].

As a case study, this work empirically explores the behavior of Snapshot-QAOA on a  $4 \times 4$  frustrated TFIM  $J_1$ - $J_2$  square lattice with periodic boundary conditions. We show that Snapshot-QAOA indeed converges towards the ground state of this TFIM with high enough QAOA layers  $p$  (Figure 1). This TFIM has known phase transitions where the ground state changes its pattern and we find that Snapshot-QAOA requires a larger circuit depth near phase transitions (Figure 4); however such circuits are still finite and achievable on near term quantum computers.

Lastly, one additional benefit to Snapshot-QAOA is its ease of implementation: it can be implemented using most already-existing QAOA software packages and libraries with little to no source code modifications.

### Related Work

Two other studies have utilized some form of QAOA to simulate quantum Hamiltonians - specifically meaning Hamiltonians with more than one Pauli basis, e.g. multi-Pauli basis, and measured expectation values in those multiple bases. The authors of [20] study depth  $p = 1$  and  $p = 2$  QAOA circuits, including on a trapped-ion quantum computer, for measuring energies of a Hamiltonian that contained both Pauli X and Y bases. This approach uses the standard variational learning loop procedure to find a set of  $\vec{\beta}, \vec{\gamma}$  that minimizes the energy of the Hamiltonian. Reference [21] numerically studies a feedback-based variant of QAOA known as FALQON [22] to simulate a 1D ANNNI (axial next-nearest-neighbor Ising) model, which contains multiple Pauli bases. The primary drawback of the feedback based FALQON algorithm is that it requires extremely high circuit depth. The work in [23] examines the task of computing low-energy states of a magnetically frustrated Hamiltonian using QAOA, including the addition of a longitudinal field. However, their Hamiltonian is still strictly diagonal. Several studies have numerically simulated QAOA based on the original motivation of QAOA, which can be viewed as a Trotterization of an adiabatic schedule; these are typically based on standard quantum annealing schedules that

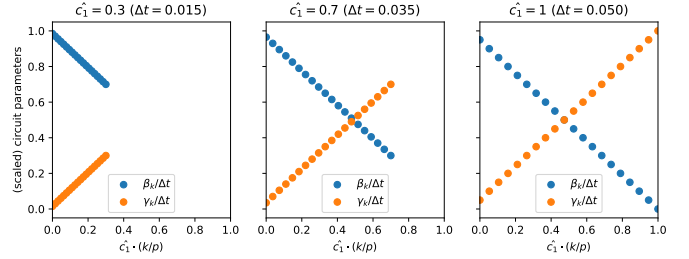


Fig. 2. A visualization connecting the  $\vec{\gamma}$  and  $\vec{\beta}$  parameters of Snapshot-QAOA to partial quantum annealing. The  $\vec{\gamma}$  and  $\vec{\beta}$  parameters of Snapshot-QAOA follow a linear ramp for varying  $\hat{c}_1$  values ( $\hat{c}_1 = 0.3, 0.7, 1.0$ ). The last subplot, with  $\hat{c}_1 = 1.0$ , corresponds to TQA [24]. Each subplot above uses  $p = 20$  layers with  $T = 1$ . The parameters are scaled by  $\Delta t = \tau/p = \hat{c}_1 T/p = \hat{c}_1/20$  so that the values along the vertical axis range lie in the interval  $[0, 1]$ . The horizontal axis represents the fraction of the total anneal schedule (from  $t = 0$  to  $t = T$ ) that the parameter corresponds to. At each  $k = 1, 2, \dots, p$ , the scaled parameters  $\beta_k/\Delta t$  and  $\gamma_k/\Delta t$  add up to 1, so the vertical axis can be interpreted as the “relative influence” that each of the two alternating unitaries has at each layer of Snapshot-QAOA.

work well at sufficiently long time evolution such as in a linear schedule [24]. While reference [24] only simulates diagonal Hamiltonians, the *long time evolution* that is a Trotterized version of the continuous time adiabatic schedule shares a similar motivation with our proposed Snapshot-QAOA.

Current analog quantum computers are able to perform similar simulations, with continuous time evolution, as Snapshot-QAOA. For example, D-Wave quantum annealers which are manufactured based on superconducting flux qubits [25, 26] can approximately simulate quantum Hamiltonians that contain  $\sum_i X_i$  terms [27–29] - this is possible since the driving Hamiltonian used in the hardware is the transverse field mixer, therefore performing state readouts during an intermediate point in the anneal can allow measurement of observables of the quantum Hamiltonian, not just the classical diagonal Hamiltonian. Programmable Rydberg atom arrays can also perform certain types of quantum Hamiltonian simulations [30, 31]. However, there are several limitations of these analog quantum simulators, such as limited qubit coherence times [32, 33], a finite measurement time that can contribute to part of the system evolution, and in the case of D-Wave quantum annealers, qubits can only be measured in the computational  $Z$ -basis.

## II. SNAPSHOT-QAOA

In this section, we go through the general theoretical framework for Snapshot-QAOA, which implements a partial quantum annealing schedule in the Quantum Approximate Optimization Algorithm (QAOA) [1]. We begin by discussing the types of Hamiltonians  $H$  that our approach can be applied to (Section II-A), then we discuss how such  $H$ 's can be viewed as a “snapshot” at some point time of an adiabatic quantum annealing schedule (Section II-B), and lastly, we provide formulae for the  $(\vec{\gamma}, \vec{\beta})$  values that correspond to a partial annealing schedule (Section II-C).

### A. General Hamiltonian Structure

In this work, we explore the problem of finding ground states and energies of certain kinds of Hamiltonians. Namely, we consider Hamiltonians  $H$  of the form:

$$H = c_0 H_0 + c_1 H_1, \quad (1)$$

where  $H_0, H_1$  are Hermitian and  $c_0, c_1 \in \mathbb{R}$ . We let  $|\psi_H\rangle$  denote the target ground state of  $H$  with corresponding ground state energy  $\mathcal{E}_H$ .

In addition to having the form above, there are five other criteria that the Hamiltonians should satisfy:

- 1) The ground state,  $|\psi_0\rangle$ , of  $H_0$  should be non-degenerate, i.e., it is the unique ground state.
- 2) The preparation of the ground state,  $|\psi_0\rangle$ , of  $H_0$  should be easily implementable on a quantum computer.
- 3) For any constant  $\alpha \in \mathbb{R}$ , the unitary operators  $e^{-i\alpha H_0}$  and  $e^{-i\alpha H_1}$  should be easily implementable on a quantum device.
- 4) The Hamiltonians  $H_0$  and  $H_1$  should not commute with one another.
- 5) For all  $T > 0$ , the corresponding time-dependent Hamiltonian with total anneal time  $T$ , i.e.,

$$\mathcal{H}_T(t) = (1 - t/T)H_0 + (t/T)H_1, \quad (2)$$

should not have any level-crossings, i.e., the two smallest eigenvalues (with multiplicity) of  $\mathcal{H}_T(t)$  have a non-zero gap between them for all  $t \in [0, T]$ .

We leave the notion of “easily implementable” up to the reader. Whether or not our approach is suitable for a particular application will depend on the specific quantum hardware, noise level tolerances, time, computing resource limits, and potentially other factors.

### B. Annealing Snapshot

Given a Hamiltonian of the form in Equation 1, we can view it as the “snapshot” of some time-dependent Hamiltonian corresponding to a linear-annealing schedule. To this end, we first construct what we call the *normalized* Hamiltonian by scaling by the appropriate factor so that the coefficients add up to 1:

$$\hat{H} = \hat{c}_0 H_0 + \hat{c}_1 H_1,$$

where,

$$\hat{c}_0 = \frac{c_0}{c_0 + c_1} \quad \text{and} \quad \hat{c}_1 = \frac{c_1}{c_0 + c_1}.$$

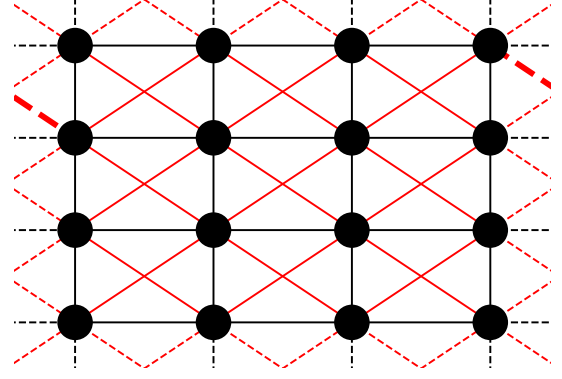


Fig. 3. The underlying graph  $G$  for the sub-Hamiltonian  $H_1$  of the  $4 \times 4$  frustrated TFIM  $H^*$  that defines toroidal periodic boundary conditions of the lattice. The black lines denote nearest-neighbor connections with weight  $J_1 = 1$  and the red lines denote next-nearest-neighbor connections with weight  $J_2$ . Each solid line corresponds to exactly one edge in  $G$ . The periodic boundary conditions are represented via dashed lines; each dashed line has a corresponding dashed line that corresponds to the same underlying edge in the graph. The bolded red lines are one such example of a pair of dashed lines that correspond to the same underlying edge.

For any  $T > 0$ , consider the corresponding time-dependent Hamiltonian with a total-anneal time of  $T$  given by Equation 2.

Observe that when substituting  $t = \hat{c}_1 T$  into the equation, then our normalized Hamiltonian  $\hat{H}$  can be viewed as a snapshot of the above Hamiltonian, i.e.,  $\hat{H} = \mathcal{H}_T(\hat{c}_1 T)$ , in other words,  $\hat{H}$  is the Hamiltonian that occurs at a  $\hat{c}_1$ -fraction of the way through the anneal process. We will use  $\tau = \hat{c}_1 T$  to denote the partial anneal time so that  $\hat{H} = \mathcal{H}_T(\tau)$ .

### C. Description of Snapshot-QAOA

Given a (quantum) Hamiltonian  $H = c_0 H_0 + c_1 H_1$  satisfying the properties in Section II-A, we now present a variant of QAOA, which we call Snapshot-QAOA, that aims to find the ground state of  $H$ . In Snapshot-QAOA with  $p$  steps, given a parameter  $T > 0$ , we construct the state

$$|\psi_p(T)\rangle = \left[ \prod_{k=1}^p \exp(-i\beta_k H_0) \exp(-i\gamma_k H_1) \right] |\psi_0\rangle,$$

where each of the  $\gamma_k$ 's and  $\beta_k$ 's are  $T$ -dependent values that are chosen in a specific way (that we will describe momentarily), and  $|\psi_0\rangle$  is the ground state of  $H_0$ . Observe that unlike standard QAOA, the phase-separating Hamiltonian  $H_1$  is *not* equal to the Hamiltonian  $H$  whose ground-state we wish to find.

In standard QAOA, by choosing  $\beta_k = \frac{T}{p} \cdot (1 - k/p)$  and  $\gamma_k = \frac{T}{p} \cdot (k/p)$ , one can show that QAOA is equivalent to a Trotterization of a linear annealing schedule with total anneal time of  $T$ ; a brief derivation of these formulas for  $\gamma_k$  and  $\beta_k$  can be found in Sack et al.'s work [24]. Since  $\hat{H} = \mathcal{H}_T(\tau)$ , the derivation can be modified to find a choice of  $(\vec{\gamma}, \vec{\beta})$  that causes Snapshot-QAOA to become a Trotterized version of a

partial annealing process running from  $t = 0$  to  $t = \tau$  of the time-dependent Hamiltonian  $\mathcal{H}_T(t)$ :

$$\begin{aligned}\beta_k &= \frac{\tau}{p} \cdot \left(1 - \frac{k\hat{c}_1}{p}\right) \\ \gamma_k &= \frac{\tau}{p} \cdot \left(\frac{k\hat{c}_1}{p}\right)\end{aligned}\quad (3)$$

Figure 2 shows how the  $\gamma_k$  and  $\beta_k$  values change (with  $k$ ) as a linear ramp. Note that  $T$  is a parameter that can be freely chosen in Snapshot-QAOA; once  $T$  (and  $p, c_0, c_1, H_0, H_1$ ) are chosen, then all the  $\beta_k$ 's and  $\gamma_k$ 's are uniquely determined. If desired, one can then choose to further optimize  $\vec{\beta}$  and  $\vec{\gamma}$  to minimize the state energy further; unless otherwise stated, we will use the term Snapshot-QAOA to refer to the algorithm *without* any further optimization of  $\vec{\gamma}$  and  $\vec{\beta}$ .

The energy  $\mathcal{E}_p(T)$  of the resulting Snapshot-QAOA state  $|\psi_p(T)\rangle$  is given by:

$$\mathcal{E}_p(T) = \langle \psi_p(T) | H | \psi_p(T) \rangle.$$

In the case that  $\tau = T$  (and hence  $\hat{c}_0 = 0$  and  $\hat{c}_1 = 1$ ), one can show that our Snapshot-QAOA method is equivalent to the method by Sack et al. which they refer to as Trotterized Quantum Annealing (TQA).

In the next few sections, we explore how Snapshot-QAOA simulations perform on certain quantum Hamiltonians of interest; for more theoretical properties of Snapshot-QAOA (e.g. periodicity, convergence, etc), we refer the interested reader to Section V.

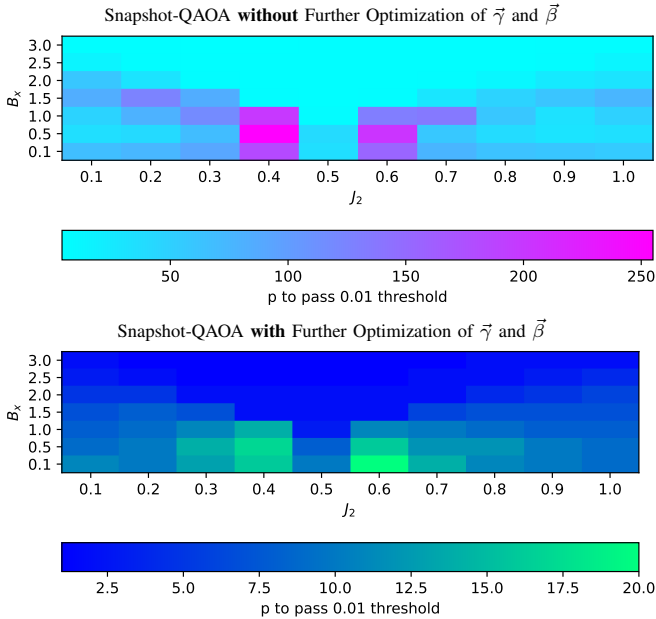


Fig. 4. Representation of the accuracy of ground-state approximation by Snapshot-QAOA, where the regions near small  $B_x$  phase transitions are hardest for Snapshot-QAOA to approximate. This accuracy is shown using a heatmap representation showing the number of  $p$  steps required for Snapshot-QAOA both with (bottom) and without (top) further optimization of the  $\vec{\gamma}$  and  $\vec{\beta}$  parameters, using  $T_{\approx}^*$ , to pass a threshold of 1% within the true ground-state  $\mathcal{E}_H$ .

### III. A TFIM TEST CASE FOR SNAPSHOT-QAOA

#### A. Transverse Field Ising Model Ground-state Simulation with Snapshot-QAOA

We now provide a class of example Hamiltonians that have the desired structure discussed in Section II-A. To that end, we turn to the Transverse Field Ising Model (TFIM) - this class of Hamiltonians contains arbitrary  $Z_i$  spin interactions, and  $\sum_i X_i$  terms. Snapshot-QAOA can address approximate ground-state finding of this general class of Hamiltonians.

Given a graph  $G = (V, E)$  with edge weights  $w : E \rightarrow \mathbb{R}$ , and a constant  $B_x$ , we can construct the following TFIM Hamiltonian:

$$H = B_x \sum_{j \in V} X_j + \sum_{(j,k) \in E} w_{jk} Z_j Z_k.$$

By identifying

$$c_0 = B_x, H_0 = \sum_{j \in V} X_j, c_1 = 1, H_1 = \sum_{(j,k) \in E} w_{jk} Z_j Z_k,$$

we see that this class of Hamiltonians adheres to the form specified in Equation 1. By normalizing the constants as is done in Section II-B, we obtain the normalized Hamiltonian  $\hat{H} = \hat{c}_0 H_0 + \hat{c}_1 H_1$  with  $\hat{c}_0 = 1 - \hat{c}_1$  where,

$$\hat{c}_1 = \frac{1}{1 + B_x}.$$

Observe that for  $B_x > 0$ , we have that  $0 < \hat{c}_1 < 1$ , thus, as discussed in Section II-B,  $\hat{H}$  can be realized as a snapshot of the annealing process of some time-dependent Hamiltonian. As a result of Section II-C, starting with the ground state of  $H_0$  (which is  $|-\rangle^{\otimes n}$ ), the ground-state of  $\hat{H}$  can be approximated using a QAOA circuit with circuit parameters set to those in Equation 3 with the substitution  $\hat{c}_1 = \frac{1}{1+B_x}$ .

#### B. Test Case: The Frustrated TFIM $J_1$ - $J_2$ Square Lattice

Here we choose a specific Hamiltonian to demonstrate the capabilities of Snapshot-QAOA; the 2D  $J_1$ - $J_2$  frustrated transverse field Ising model [34–36]:

$$H = -J_1 \sum_{NN} Z_j Z_k + J_2 \sum_{NNN} Z_j Z_k + B_x \sum_j X_j, \quad (4)$$

where  $NN$  defines the set of nearest neighbors in Euclidean space, and  $NNN$  defines the corresponding set of next-nearest-neighbors. This model has competing magnetic interactions between the ferromagnetic nearest neighbor terms and the next-nearest-neighbor terms which are antiferromagnetic favouring stripe like patterns. We set  $J_1 = 1$  and then vary  $J_2$  as the frustration parameter. This Hamiltonian serves as a good test case for the simulation capabilities of Snapshot-QAOA because it is geometrically frustrated and contains a phase transition at the critical point of  $J_2 = 0.5$  for small  $B_x$ . The Hamiltonian used in the numerical simulations below has a graph  $G$  that is a  $4 \times 4$  grid with periodic boundary conditions where the edge to each vertex's nearest neighbor (i.e. the 4

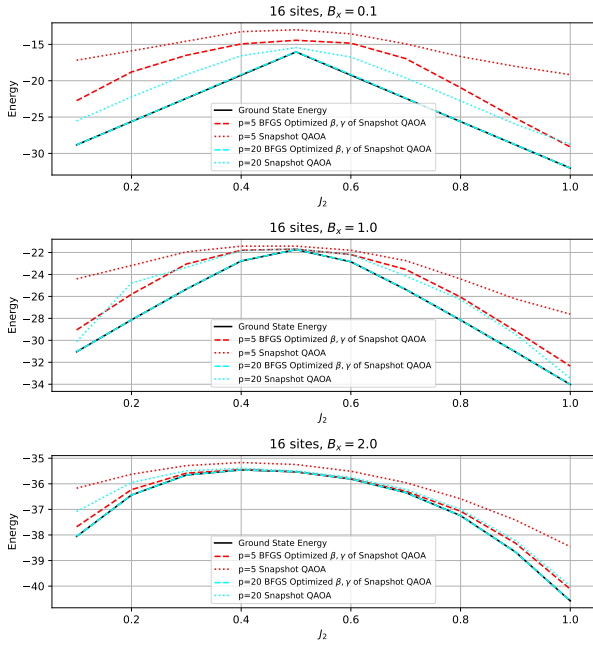


Fig. 5. Energies returned by Snapshot-QAOA with (dashed lines) and without (dotted lines) further optimization of the  $\gamma$  and  $\beta$  parameters using BFGS, compared to the exact ground truth energy (solid black line). Each curve color (other than black) corresponds to a different  $p$  value, for  $p = 5$  (red) and  $p = 20$  (cyan). Each subplot corresponds to a different  $B_x$  value, with the  $x$ -axis denoting varying values of  $J_2$  and the  $y$ -axis corresponding to energy values. Each Snapshot-QAOA run is performed using the approximate optimal total anneal time of  $T_{\approx}^*$ .

neighbors in each of the 4 cardinal directions) has weight  $J_1$  and the edge to each vertex's next-nearest neighbor (i.e. the 4 neighbors that are immediately diagonal to the vertex in the grid) has weight  $J_2$ ; a depiction of this graph can be found in Figure 3. We will denote this specific Hamiltonian as  $H^*$  or as  $H^*(J_2, B_x)$  when we wish to refer to the Hamiltonian with specific  $J_2$  and  $B_x$  values.

Exact classical methods are limited to small system sizes while statistical methods like Monte Carlo methods can only simulate the ground state properties at non-zero temperature limit [37]. Thus, these methods are not suitable ground state properties of physical systems in zero-temperature limit where quantum effects are the strongest. Approximate classical methods like Density Matrix Renormalization Group (DMRG) are optimized for cylindrical boundary conditions [38] unlike the toroidal geometry (see Figure 3) of the problem discussed in our work. Therefore, we investigate the quantum algorithm Snapshot-QAOA to obtain approximate ground-states of this system.

#### IV. NUMERICAL RESULTS

We present numerical simulations of Snapshot-QAOA on a specific test case of a frustrated lattice defined by the Hamiltonian  $H^*$  in Section III. All numerical simulations are performed using an adapted version of the Julia programming language [39] based QAOA simulator `JuliaQAOA` [40]. All numerical experiments use statevector simulations; no shot

noise is present. All eigenstates of 16-qubit Hamiltonians are computed through LAPACK based exact diagonalization routines in Python programming language [41]. This method gives us exact ground state energy  $\mathcal{E}_H$  for benchmarking purposes. We also obtain the information about energy gap to the excited states. Some results will consider Snapshot-QAOA with further optimization of the  $\vec{\gamma}$  and  $\vec{\beta}$  parameters; in such cases further optimization is done via a local search using the gradient-based Broyden-Fletcher-Goldfarb-Shanno (BFGS) optimizer [42] with  $\vec{\gamma}$  and  $\vec{\beta}$  initialized according to Equation 3.

As an initial clear finding, Figure 1 shows that Snapshot-QAOA converges to the ground-state energy of quantum Hamiltonians. The following plots in this section examine various additional properties of Snapshot-QAOA.

For different fixed values of  $J_2$  and  $B_x$ , we investigate the behavior of the convergence of the Snapshot-QAOA energy  $\mathcal{E}_p(T)$  as  $p$  changes if an approximate optimal  $T_{\approx}^*$  is used (where  $T_{\approx}^*$  is obtained from a heuristic to be described later). In the case that the true optimal total annealing time  $T^*$  is used, the convergence is guaranteed as  $\lim_{p \rightarrow \infty} \min_{T \in \mathbb{R}} \mathcal{E}_p(T) = \mathcal{E}_H$  (which we later prove in Section V-A).

Figure 1 shows the convergence of energy as a function of  $p$  for several different Hamiltonian parameters using Snapshot-QAOA, and Figure 6 shows a similar representation for when  $\vec{\beta}, \vec{\gamma}$  is optimized using BFGS. Importantly, regardless of whether or not  $\vec{\gamma}$  and  $\vec{\beta}$  are further optimized, the energy does not always monotonically improve as a function of  $p$  - cases where the energy gets worse are marked with vertical cyan lines or triangles. These  $p$  steps where there is a lack of improvement is not advantageous - for example ideally these steps would be skipped if this is a characteristic even for globally optimal  $T$  and this could be known a-priori. It is an open question whether monotonic improvement in  $p$  is always expected for Snapshot-QAOA if the globally optimal  $T^*$  parameter is found, or whether this is a consequence of the heuristic used to obtain  $T_{\approx}^*$ . Importantly, the optimization of  $T$  in Figure 1 is *not* a global optimization over the entire  $T$  parameter space and therefore does not answer whether consistent improvement is always expected. Notably however, for some parameter values there is *always* a consistent improvement of energy. The most important feature of the plots in Figure 1 is that Snapshot-QAOA (without further optimization of  $\vec{\gamma}$  and  $\vec{\beta}$ ) has energies that tend to converge to the ground-state energy within 100 steps of  $p$ ; meanwhile, in Figure 6, convergence towards the ground-state energy tends to occur within 20 steps of  $p$  when we do allow for further optimization of  $\vec{\gamma}$  and  $\vec{\beta}$ .

A natural question is how Snapshot-QAOA (with and without further optimization of  $\vec{\gamma}$  and  $\vec{\beta}$ ) depends on  $p$ , as well as the frustrated Hamiltonian parameters  $J_2, B_x$ . We address this by measuring the number of  $p$  steps required to reach a certain accuracy threshold within the true ground-state energy. Figure 4 plots the number of  $p$  steps required to reach an energy that is within 1% of the ground-state energy

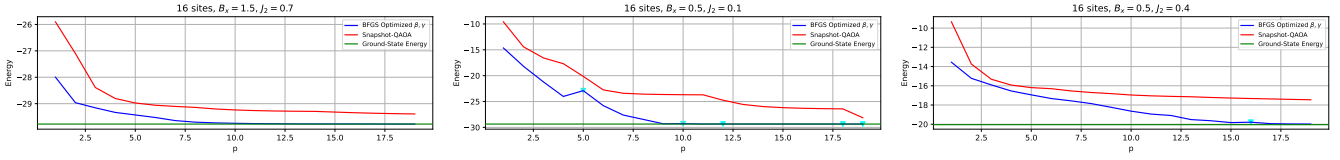


Fig. 6. Further optimization of  $\vec{\gamma}$  and  $\vec{\beta}$  using BFGS, starting from the  $T_{\approx}^*$  Snapshot-QAOA angles, for  $p = 1$  up to  $p = 20$ . Energy (y-axis) as a function of  $p$  (x-axis), where the known ground-state energy  $\mathcal{E}_H$  is marked by a green horizontal line. Red line shows the Snapshot-QAOA energy from having only optimized  $T$  and found  $T_{\approx}^*$ . Blue line shows the energy of the Hamiltonian after BFGS has optimized the vectors of QAOA angles  $\vec{\gamma}$  and  $\vec{\beta}$ , where those angles are initialized from the  $T_{\approx}^*$  angles. Cyan triangles on the blue line denote any  $p + 1$  indices where there is a decrease in performance (i.e. an increase in energy) compared to the previous  $p$ . These results show that further optimization of  $\vec{\gamma}$  and  $\vec{\beta}$  can substantially improve the energy obtained from Snapshot-QAOA.

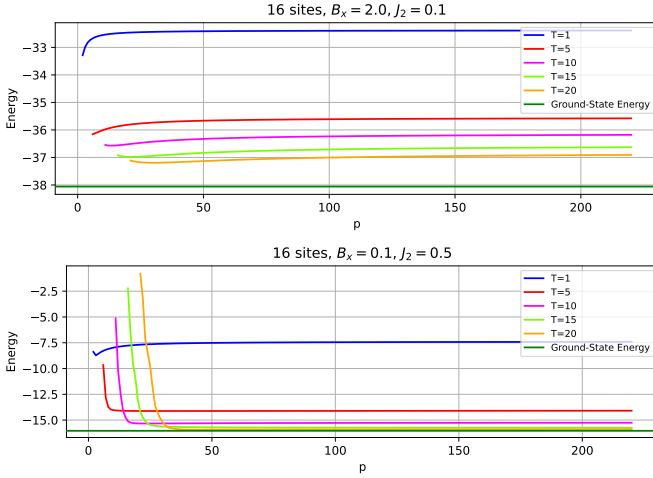


Fig. 7. Fixed  $T$  with varying  $p$  (x-axis) and resulting energy (y-axis) for two representative Hamiltonian parameters. Green horizontal line denotes the ground-state energy  $\mathcal{E}_H$ .

of the Hamiltonian  $H^*(J_2, B_x)$  using Snapshot-QAOA with and without further optimization of  $\vec{\gamma}$  and  $\vec{\beta}$ . Remarkably, this representation of the complexity search space to approximate the ground-state of this frustrated model uncovers a reasonably accurate representation of the magnetic phase diagram of this model [34, 35]. Namely, the paramagnetic phase, also referred to as the  $\Gamma$ -phase, requires the smallest number of  $p$  steps to approximate the ground-state, shown by the cyan region in Figure 4. Whereas, the ferromagnetic and antiferromagnetic stripe phase regions on either side of  $J_2 = 0.5$  at smaller  $B_x$  values require the largest  $p$  steps, with the ferromagnetic region requiring the most  $p$  steps.

Notably, when further optimization of  $\vec{\gamma}$  and  $\vec{\beta}$  are allowed, Snapshot-QAOA was able to reach good approximation within only 20  $p$  steps for all evaluated regions of the Hamiltonian parameter space, whereas Figure 4 (top) shows that Snapshot-QAOA without such further optimization, while it does converge, required up to 250  $p$  steps.

In Figure 5, the Snapshot-QAOA energies (both with and without further optimization of  $\vec{\gamma}$  and  $\vec{\beta}$ ) and the exact ground state energies are plotted together, with different energy curves for varying values of  $p$ . Similar to what was observed in Figure 4, in Figure 5 it is clear that the energies produced by Snapshot-QAOA converge to the true ground state energy

much faster whenever further optimization of  $\vec{\gamma}$  and  $\vec{\beta}$  is allowed.

Recall that the total anneal time  $T$  is a Snapshot-QAOA parameter that needs to be chosen. Ideally, one would use the ( $p$ -dependent) optimal  $T^*$  which is non-trivial to find. For the simulations yielding the results of Figure 4, we use a simple heuristic to obtain an estimate  $T_{\approx}^*$  of the best total anneal time; these  $T_{\approx}^*$  values are used for both versions of Snapshot-QAOA (both with and without further optimization of  $\vec{\gamma}$  and  $\vec{\beta}$ ). In the remaining subsections, we discuss and provide results regarding the influence that the parameter  $T$  has on Snapshot-QAOA, restricting our attention now to the case where  $\vec{\gamma}$  and  $\vec{\beta}$  are not further optimized by the BFGS algorithm.

#### A. Behavior of $\mathcal{E}_p(T)$ with $T$ fixed

Figure 7 depicts how the energy  $\mathcal{E}_p(T)$  changes with  $p$ , with each curve representing a different fixed value of  $T$ . There are a few key observations. First, we observe that each curve appears to be converging to some fixed value; this is expected as  $\lim_{p \rightarrow \infty} \mathcal{E}_p(T)$  converges to the energy  $\mathcal{E}_{QA}(T)$  obtained by quantum annealing which we later discuss in Section V-A. We remark that such curves are not necessarily monotonically decreasing. For large enough  $p$  (i.e. the right-most parts of the figure), we see that increasing  $T$  brings the energy closer<sup>1</sup> to the ground state energy  $\mathcal{E}_H$ ; again, this is as expected as  $\lim_{T \rightarrow \infty} \mathcal{E}_{QA}(T) = \lim_{T \rightarrow \infty} \lim_{p \rightarrow \infty} \mathcal{E}_p(T) = \mathcal{E}_H$  as discussed later in Section V-A. However, looking at the left-most parts of each sub-plot, we observe that increasing  $T$  does not necessarily yield a better energy; this motivates investigating how to find the optimal  $T$  for any fixed  $p$ , which we do in the next subsection.

#### B. Optimizing $T$ with Fixed $p$

In the adiabatic quantum annealing setting, due to the quantum adiabatic theorem, one is guaranteed to obtain the ground state in the limit as  $T \rightarrow \infty$ . However, in our QAOA setting with a fixed choice of  $p$ , this is no longer the case due to the fact that as  $T$  increases, so does the step-size

<sup>1</sup>The right side of each sub-plot of Figure 7 seems to suggest that  $\mathcal{E}_{QA}(T)$  is monotonically decreasing in  $T$ ; however, we do not claim that this is always the case as the adiabatic theorem only guarantees a limiting behavior and not a monotonic behavior. Prior work has shown for success probabilities (an alternative metric of success), that there is non-monotonic behavior with changing  $T$  [43].

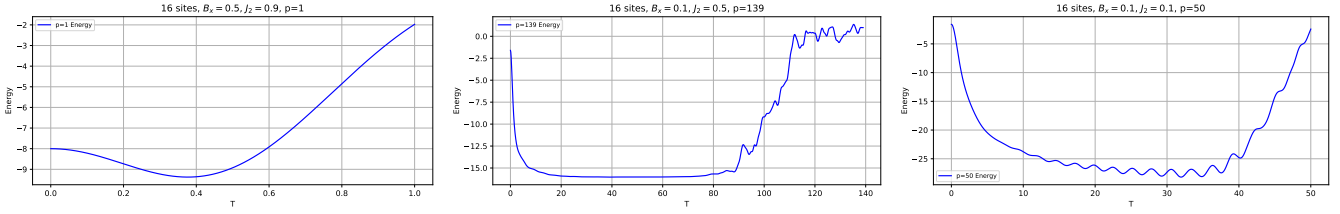


Fig. 8. Zoom in on  $[0, p]$   $T$  parameter search space. Several examples of the energy of the Hamiltonian (y-axis) vs. the total-anneal-time parameter  $T$  (x-axis), for different values of  $p$ ,  $J_2$ , and  $B_x$ . Each plot is showing the Hamiltonian expectation value for 1000 linearly spaced  $T$  values between 0 and  $p$ .

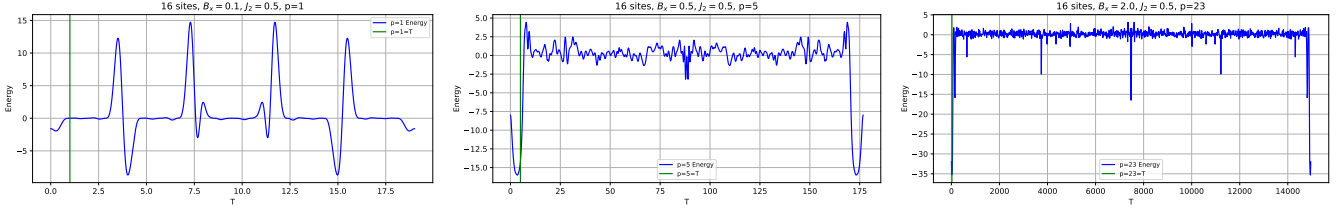


Fig. 9. Several examples of the energy of the Hamiltonian (y-axis) vs. the total-anneal-time parameter  $T$  (x-axis), for different values of  $p$ ,  $J_2$ , and  $B_x$ . Each plot is showing the Hamiltonian expectation value for 1000 linearly spaced  $T$  values between 0 and the minimum  $T$ -period  $\rho$ . The x-axis index where  $T = p$  is marked by a vertical green line. Notice that there is a clear mirror symmetry in each  $T$  search space.

$\Delta t = \tau/p = \hat{c}_1 T/p$ , leading to an increase in Trotterization errors. The fixed  $p$  regime is of interest since increased  $p$  leads to increased circuit depth (and hence increased runtime and quantum decoherence/noise), whereas, interestingly, the total annealing time  $T$  has no (direct) effect on the circuit depth of Snapshot-QAOA.

Sack et al. [24] explored this phenomena in TQA setting (i.e.  $\tau = T$ ) in the context of 3-regular Max-Cut. Similar to Sack et al., we found that Snapshot-QAOA on our Hamiltonian  $H^*$  of interest had an energy-minimizing  $T$  in the range of  $[0, p]$  as seen in Figure 8 which plots overall anneal time  $T$  vs the energy  $\mathcal{E}_p(T)$  for  $T \in [0, p]$ . In Figure 8 (left), we see the same phenomena observed by Sack et al. [24] where as  $T$  increases, the energy monotonically decreases to some minima before starting to increase again. However, by changing  $J_2, B_x$ , and  $p$ , we sometimes observe slightly different behavior. For example, in Figure 8 (right), there are small, rapid oscillations in the overall “dip” in the plot; such oscillations may make it difficult to optimize using certain optimization methods (e.g. gradient descent), in particular for larger  $p$  if the landscape contains many more oscillations. Another example is Figure 8 (center) where the minimum (over  $[0, p]$ ) appears to lie in a sort of plateau and the plot has a more unpredictable and erratic behavior for  $T \in [p/2, p]$ .

Given the results above where  $T \in [0, p]$ , one may think that as  $T$  increases (beyond  $T > p$ ) that the energy becomes increasingly worse due to the increased proliferation of Trotter-like errors. However, we will later prove in Section V-B that this cannot possibly be the case since the energy is periodic in  $T$  (with the period  $\rho$  given by Equation 5). This warrants further investigation, in particular, it is not clear what the behavior of the  $T$ -vs-Energy curve is past  $T > p$  and it is not clear a priori if the optimal  $T^*$  always lies in or near the interval  $[0, p]$ .

In Figure 9, we show plots for several values of  $p, B_x, J_2$ , illustrating the diversity in behavior of the energy as  $T$  changes throughout its period; in particular, it can be observed that as  $p$  increases, so does the number of sudden sharp peaks and valleys in the energy curve over the period  $\rho$ . This shows that in principle, in order to find the globally optimal  $T^*$ , we would need to perform an exhaustive search over the interval  $[0, \rho]$ , or more precisely  $\frac{\rho}{2}$  because the energy landscape has a mirror symmetry. This is important to note because  $\rho$  can grow to be substantially large. We also replicate and extend Sack et al.’s work, extending the inset figure of Figure 3 of [24] to larger  $T$  values in Figure 10 ; as a result we also find the same complex relationship between  $T$  and the energy for TQA (i.e. the  $\tau = T$  setting).

In Figure 9, we highlight a specific plot (with  $p = 1, J_2 = 0.5, B_x = 0.1$ ) where the optimal  $T^*$  is not close to being in the interval  $[0, p]$ . This shows that looking in the interval  $T \in [0, p]$  is not always sufficient if one wishes to find  $T^*$ .

Due to the challenges above, one can imagine various methods for optimizing  $T$  with differing trade-offs between accuracy and runtime. One (expensive) option is to perform a fine grid-search over the entire period  $\rho$ ; however, this is prohibitive since the size of the period  $\rho$  grows very quickly with  $p$  as illustrated in Figure 11. Alternatively, one could perform a fine grid-search over a small interval in the beginning of the period; this is what we do for the results in this work to approximate the optimal  $T^*$  value. More specifically, we do a grid-search over the interval  $T \in [0, p]$  with a step-size of  $\Delta T = 0.01$ ; we denote the approximate optimal  $T$  found by this procedure as  $T_{\approx}^*$ .

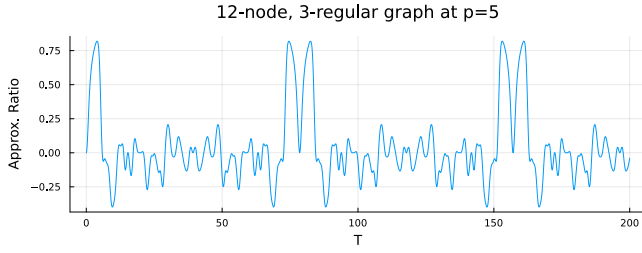


Fig. 10. The approximation ratio ( $y$ -axis) obtained by TQA (i.e. Snapshot-QAOA with  $\tau = T$ ) for varying values of  $T$  ( $x$ -axis) on a 12-node 3-regular graph with  $p = 5$  layers. The approximation ratio is defined in the same (non-traditional) manner as in [24]; where they use  $H = \sum_{(i,j) \in E} Z_i Z_j$  (instead of  $H = \sum_{(i,j) \in E} \frac{1}{2}(1 - Z_i Z_j)$ ) for the Max-Cut Hamiltonian and the approximation is given by  $\langle \psi(T) | H | \psi(T) \rangle / \mathcal{E}_H$  where  $|\psi(T)\rangle$  is the output of the algorithm with parameter  $T$  and  $\mathcal{E}_H$  is the ground state energy of  $H$ .

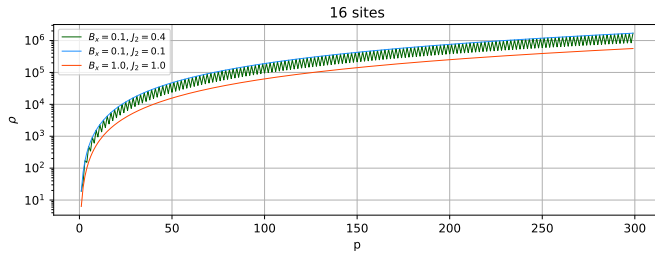


Fig. 11. Scaling of the minimum  $T$  period  $\rho$  ( $y$ -axis) as a function of  $p$  ( $x$ -axis) for several representative Hamiltonian parameter choices of  $J_2$  and  $B_x$ . Log scale on the  $y$ -axis. This shows that  $\rho$ , and therefore in principle the maximum size of the  $T$  search space, grows quite quickly as a function of  $p$ .

### C. Linear Regression Between $T^*$ and $p$ in the Interval from $[0, p]$

In the case of TQA (i.e. Snapshot-QAOA with  $\tau = T$ ) for the 3-regular Max-Cut problem, Sack et al. [24] found that the relationship between  $p$  and the optimal  $T^*$  is approximately linear; in particular, they empirically show that  $T^* \approx \delta t \cdot p$  where  $\delta t \approx 0.75$ .

For general Snapshot-QAOA, if a linear-relationship strongly holds for all  $T^*$  and  $p$  and we have an accurate estimate of the “slope”  $\delta t$ , then this gets around the challenges regarding finding the optimal  $T^*$  as discussed in Section IV-B. In the rest of this section, we investigate the relationship between  $T^*$  and  $p$  to see if any such linear relationship exists. Since the true  $T^*$  is challenging to obtain and verify (as discussed in Section IV-B), we instead work with the estimate  $T_{\approx}^*$ .

In Figure 12, we show the results of the linear regression (and the underlying data) for 4 different choices of  $(J_2, B_x)$  between  $p$  and  $T_{\approx}^*$ . In some cases, e.g. Figure 12 (top-right), we find a nearly perfect linear relationship. In other cases, e.g. Figure 12 (bottom-left), the linear relationship is much weaker but with the overall trend still appearing roughly linear. Meanwhile, Figure 12 (bottom-right) shows that there exist cases where the relationship between  $T_{\approx}^*$  and  $p$  has bizarre behavior, with large jumps and long plateaus. These results

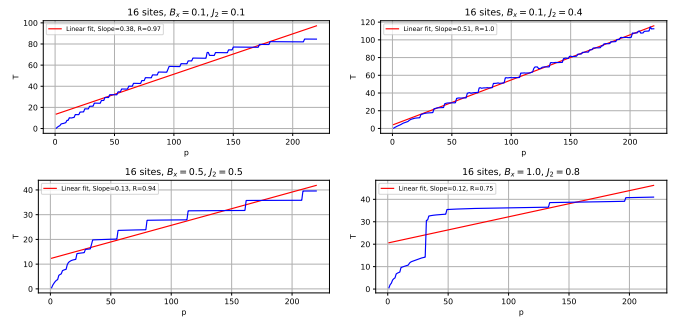


Fig. 12. Linear regression between  $p$  ( $x$ -axis) and  $T_{\approx}^*$  ( $y$ -axis), for all steps of  $p$  up to  $p = 220$ . All of these relationships appear to be approximately stepwise functions, but the step size is not consistent. Some of the step sizes are small enough that the linear function approximates the relationship well, whereas for others the relationship is much weaker.

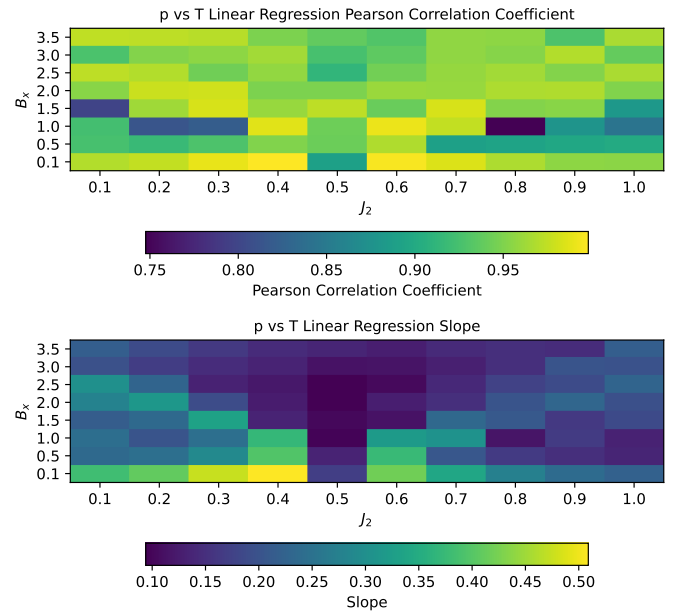


Fig. 13. Heatmaps of linear regression quantities between  $p$  and  $T_{\approx}^*$  from  $p = 1$  up to  $p = 220$ . Pearson correlation coefficient  $R$  (top) and slope (bottom).

mean that for some parameters, a reasonably simple linear extrapolation could find good values of  $T_{\approx}^*$ , but in general the results indicate that more complex extrapolations would be required – and in particular the relationship between  $p$  and  $T_{\approx}^*$  depends on the underlying Hamiltonian being simulated.

In Figure 13, we provide a heatmap that shows how the slope  $\delta t$  (calculated via linear regression) changes with changing  $J_2$  and  $B_x$ . Additionally, we provide a similar heatmap showing the  $R$  coefficient of the linear regression. Notably, the heatmap of the slope  $\delta t$  appears to approximately recover the search space of the magnetic phases of the underlying frustrated  $J_1$ - $J_2$  model [34, 35], just as the accuracy threshold plot of Figure 4 did.



## V. ANALYTICAL RESULTS

In this section, we present theoretical results regarding how the energy  $\mathcal{E}_p(T)$  (of the state  $|\psi_p(T)\rangle$ ) output by Snapshot-QAOA changes as  $p$  and  $T$  vary. Section V-A gives us assurance that the ground energy is approached as  $p$  tends to infinity. Section V-B shows that the parameter search space for  $T$  can typically be restricted to a bounded region that can easily be calculated.

### A. Limiting Behavior as $T \rightarrow \infty$ and $p \rightarrow \infty$

Let  $\mathcal{E}_{\text{QA}}(T) = \lim_{p \rightarrow \infty} \mathcal{E}_p(T)$ ; then  $\mathcal{E}_{\text{QA}}(T)$  is the result of the Trotter limit which is exactly equal to the energy achieved by doing quantum annealing with time-dependent Hamiltonian  $\mathcal{H}_T$  (from time  $t = 0$  to  $t = \tau$ ). Since the corresponding time-dependent Hamiltonian  $\mathcal{H}_T$  is assumed to not have any level-crossings, it then follows from the quantum adiabatic theorem that  $\lim_{T \rightarrow \infty} \mathcal{E}_{\text{QA}}(T) = \lim_{T \rightarrow \infty} \lim_{p \rightarrow \infty} \mathcal{E}_p(T) = \mathcal{E}_H$ , i.e., one achieves the ground state energy of  $H$  in the limit. We remark that the ordering of the limits ( $\lim_{T \rightarrow \infty}$ ) and ( $\lim_{p \rightarrow \infty}$ ) is important; in particular  $\lim_{p \rightarrow \infty} \lim_{T \rightarrow \infty} \mathcal{E}_p(T)$  is undefined since  $\lim_{T \rightarrow \infty} \mathcal{E}_p(T)$  will typically not exist (see Figure 9). However, what can be said is that  $\lim_{p \rightarrow \infty} \min_{T \in \mathbb{R}} \mathcal{E}_p(T) = \mathcal{E}_H$ ; this can easily be shown via the squeeze theorem of calculus:

$$\begin{aligned} \mathcal{E}_H &\leq \min_{T'} \mathcal{E}_p(T') \leq \mathcal{E}_p(T), \quad \forall p, \forall T, \\ \implies \mathcal{E}_H &\leq \lim_{p \rightarrow \infty} \min_{T'} \mathcal{E}_p(T') \leq \lim_{p \rightarrow \infty} \mathcal{E}_p(T), \quad \forall T \\ \implies \mathcal{E}_H &\leq \lim_{p \rightarrow \infty} \min_{T'} \mathcal{E}_p(T') \leq \lim_{T \rightarrow \infty} \lim_{p \rightarrow \infty} \mathcal{E}_p(T) = \mathcal{E}_H \\ &\implies \lim_{p \rightarrow \infty} \min_{T'} \mathcal{E}_p(T) = \mathcal{E}_H. \end{aligned}$$

### B. Periodicity of $T$

Suppose that the QAOA unitaries corresponding to  $H_0$  and  $H_1$  are both periodic in  $\beta$  and  $\gamma$ , i.e.,  $e^{-i\beta H_0}$  is periodic in  $\beta$  with period  $\rho_0$  and  $e^{-i\gamma H_1}$  is periodic in  $\gamma$  with period  $\rho_1$ . Then, unlike the quantum annealing case, it can be shown that the energy of Snapshot-QAOA is periodic in  $T$  with a period  $\rho$  that can be easily calculated, i.e.,  $\mathcal{E}_p(T) = \mathcal{E}_p(\rho + T)$  for all  $T$ . For the period  $\rho$  that we calculate below, we do not make any claims regarding whether or not such a  $\rho$  is a *minimal* period or not.

For  $k = 1, 2, \dots, p$ , let  $\hat{\beta}_k$  and  $\hat{\gamma}_k$  be the values that partial-annealing QAOA would return in the case that  $T = 1$ . Observe that if  $\beta_k$  and  $\gamma_k$  are the values returned by partial-annealing QAOA for arbitrary  $T$ , then  $\beta_k = T\hat{\beta}_k$  and  $\gamma_k = T\hat{\gamma}_k$  (this follows from how  $\gamma_k$  and  $\beta_k$  are defined in Equation 3). It then follows that the QAOA unitary  $e^{-i\beta_k H_0} = e^{-i\hat{\beta}_k T H_0}$  is periodic in  $T$  with period  $\rho_0/\hat{\beta}_k$  and similarly,  $e^{-i\gamma_k H_1} = e^{-i\hat{\gamma}_k T H_1}$  is periodic in  $T$  with period  $\rho_1/\hat{\gamma}_k$ . Thus, as a function of  $T$ , the overall state (and hence the energy) of Snapshot-QAOA has a period that is the least-common multiple (LCM) of periods of each unitary, i.e.,

$$\rho = \text{LCM}(\rho_0/\hat{\beta}_1, \dots, \rho_0/\hat{\beta}_p, \rho_1/\hat{\gamma}_1, \dots, \rho_1/\hat{\gamma}_p). \quad (5)$$

It can also be shown that *within* each period  $\rho$ , there exists a mirror-symmetry, i.e.,  $\mathcal{E}_p(T) = \mathcal{E}_p(\rho - T)$ . From Equation 3, it is clear that the anneal time from  $T$  to  $-T$  has the effect of negating all of the  $\gamma_k$  and  $\beta_k$  parameters, which is known to not have an effect on energies output by the QAOA circuit (see [44] for an elegant proof). Thus,  $\mathcal{E}_p(T) = \mathcal{E}_p(-T) = \mathcal{E}_p(\rho - T)$  for all  $T$ .

We remark that in the case where  $H_0$  is the transverse field mixer, i.e.,  $H_0 = -\sum_j X_j$ , then  $\rho_0 = \pi/2$  is a minimum period. In the case that  $H_1$  is a diagonal matrix with integer entries, then one can take  $\rho_1 = 2\pi$ . For the specific Hamiltonian  $H^*(J_2, B_x)$  defined in Section III-B, if  $J_2 = \frac{a}{b} \in \mathbb{Q}$  is written as a reduced-fraction, then one can take  $\rho_1 = b \cdot (\pi/2)$ .

## VI. DISCUSSION

This study has proposed an extension of QAOA that allows approximate ground-state finding of Hamiltonians that contain  $\sum_i X_i$  terms, using QAOA driven by that transverse field. We have shown that Snapshot-QAOA can approximate the ground-state of quantum Hamiltonians very well, as evidenced by numerical simulations of a frustrated 2D  $J_1$ - $J_2$  TFIM model in various regions of its magnetic phase diagram. Importantly, Snapshot-QAOA is quite NISQ-hardware friendly (Noisy Intermediate Scale Quantum [45]) - and can be used without any variational learning procedure, or optionally can be further optimized using variational learning.

In theory, other mixing Hamiltonians could satisfy the required properties of Snapshot-QAOA - and therefore the ground states of more complex quantum Hamiltonians could also be approximated, not just transverse field driven systems. Such Hamiltonians would require more circuit complexity to go into the implementation of the mixing unitary; one advantage of the transverse field mixer is that the circuit complexity is only a single layer of single qubit gates per  $p$ . It may also be of interest to study Hamiltonians for which the partial annealing time  $\tau$  is “nonphysical”, i.e.,  $\tau \notin [0, T]$ .

One of the most important future topics of study for Snapshot-QAOA is determining more sophisticated methods of approximating optimal  $T$ , and moreover determining under what conditions the optimal  $T$  is within the range  $[0, p]$  and under what conditions that is not the case. Another open question is understanding the full complexity of the search landscapes of  $T$ . What is clear is that optimizing  $T$  is easier than directly optimizing  $\vec{\gamma}$  and  $\vec{\beta}$  in the sense that  $T$  contains fewer tunable parameters, namely being the sole parameter, whereas the full set of (standard) QAOA angles contains  $2p$  parameters. Another open question is how much performance can be gained by heavily optimizing the  $\vec{\beta}$ ,  $\vec{\gamma}$  from Snapshot-QAOA compared to only using optimized  $T^*$  and if these optimized values of  $\vec{\beta}$  and  $\vec{\gamma}$  are amenable to parameter transfer; it is known for standard QAOA that optimized parameters are indeed transferable [46–51], (this is also known as parameter concentration [52]).

For the particular Snapshot-QAOA simulations we performed on the frustrated  $J_1$ - $J_2$  TFIM model, there are several

open questions. The clearest open question is why Snapshot-QAOA is able to efficiently, with a small number of  $p$  steps, approximate the system at the phase transitions for small  $B_x$  and  $J_2 = 0.5$  – but also requires a large number of  $p$  steps for the states very near (but not *at*) these phase transitions. Another open question is why the linear regression slopes and  $p$  steps to pass certain accuracy thresholds both approximately replicate the regions of the underlying magnetic phase diagram of the model (Figures 4, 13).

Lastly, it would be an interesting question to consider how Snapshot-QAOA could be used as an initial state for QPE [19].

#### ACKNOWLEDGMENTS

This work was supported by the U.S. Department of Energy through the Los Alamos National Laboratory. Los Alamos National Laboratory is operated by Triad National Security, LLC, for the National Nuclear Security Administration of U.S. Department of Energy (Contract No. 89233218CNA000001). Research presented in this article was supported by the NNSA’s Advanced Simulation and Computing Beyond Moore’s Law Program at Los Alamos National Laboratory and by the Laboratory Directed Research and Development program of Los Alamos National Laboratory under project number 20230049DR. This research used resources provided by the Darwin testbed at Los Alamos National Laboratory (LANL) which is funded by the Computational Systems and Software Environments subprogram of LANL’s Advanced Simulation and Computing program (NNSA/DOE). LA-UR-24-33288.

## REFERENCES

- [1] Edward Farhi, Jeffrey Goldstone, and Sam Gutmann. “A Quantum Approximate Optimization Algorithm”. In: *arXiv preprint* (Nov. 2014). DOI: [10.48550/ARXIV.1411.4028](https://doi.org/10.48550/ARXIV.1411.4028). arXiv: [1411.4028](https://arxiv.org/abs/1411.4028). URL: <https://doi.org/10.48550/arXiv.1411.4028>.
- [2] Edward Farhi, Jeffrey Goldstone, and Sam Gutmann. “A Quantum Approximate Optimization Algorithm Applied to a Bounded Occurrence Constraint Problem”. In: *arXiv preprint* (June 2015). DOI: [10.48550/arXiv.1412.6062](https://doi.org/10.48550/arXiv.1412.6062). arXiv: [1412.6062](https://arxiv.org/abs/1412.6062). URL: <https://doi.org/10.48550/arXiv.1412.6062>.
- [3] Stuart Hadfield et al. “From the Quantum Approximate Optimization Algorithm to a Quantum Alternating Operator Ansatz”. In: *Algorithms* 12.2 (2019), p. 34. DOI: [10.3390/a12020034](https://doi.org/10.3390/a12020034). arXiv: [1709.03489](https://arxiv.org/abs/1709.03489). URL: <https://doi.org/10.3390/a12020034>.
- [4] Ruslan Shaydulin et al. “Evidence of scaling advantage for the quantum approximate optimization algorithm on a classically intractable problem”. In: *Science Advances* 10.22 (May 2024), eadm6761. DOI: [10.1126/sciadv.adm6761](https://doi.org/10.1126/sciadv.adm6761). arXiv: [2308.02342](https://arxiv.org/abs/2308.02342).
- [5] John Golden et al. “Numerical Evidence for Exponential Speed-up of QAOA over Unstructured Search for Approximate Constrained Optimization”. In: *IEEE International Conference on Quantum Computing and Engineering QCE'23*. Sept. 2023, pp. 496–505. DOI: [10.1109/QCE57702.2023.00063](https://doi.org/10.1109/QCE57702.2023.00063). arXiv: [2202.00648](https://arxiv.org/abs/2202.00648).
- [6] Sami Boulebnane and Ashley Montanaro. “Solving Boolean Satisfiability Problems With The Quantum Approximate Optimization Algorithm”. In: *PRX Quantum* 5 (3 Sept. 2024), p. 030348. DOI: [10.1103/PRXQuantum.5.030348](https://doi.org/10.1103/PRXQuantum.5.030348). arXiv: [2208.06909](https://arxiv.org/abs/2208.06909).
- [7] Ashley Montanaro and Leo Zhou. “Quantum speedups in solving near-symmetric optimization problems by low-depth QAOA”. In: (2024). arXiv: [2411.04979](https://arxiv.org/abs/2411.04979) [quant-ph]. URL: <https://arxiv.org/abs/2411.04979>.
- [8] Zhihui Wang et al. “XY mixers: Analytical and numerical results for the quantum alternating operator ansatz”. In: *Phys. Rev. A* 101 (1 2020), p. 012320. DOI: [10.1103/PhysRevA.101.012320](https://doi.org/10.1103/PhysRevA.101.012320). URL: <https://link.aps.org/doi/10.1103/PhysRevA.101.012320>.
- [9] Andreas Bartschi and Stephan Eidenbenz. “Grover Mixers for QAOA: Shifting Complexity from Mixer Design to State Preparation”. In: *2020 IEEE International Conference on Quantum Computing and Engineering (QCE)*. IEEE, Oct. 2020, 72–82. DOI: [10.1109/qce49297.2020.00020](https://doi.org/10.1109/qce49297.2020.00020). URL: <http://dx.doi.org/10.1109/QCE49297.2020.00020>.
- [10] Zichang He et al. “Alignment between initial state and mixer improves QAOA performance for constrained optimization”. In: *npj Quantum Information* 9.1 (Nov. 2023). ISSN: 2056-6387. DOI: [10.1038/s41534-023-00787-5](https://doi.org/10.1038/s41534-023-00787-5). URL: <http://dx.doi.org/10.1038/s41534-023-00787-5>.
- [11] Reuben Tate et al. “Warm-Started QAOA with Custom Mixers Provably Converges and Computationally Beats Goemans-Williamson’s Max-Cut at Low Circuit Depths”. In: *Quantum* 7 (2023), p. 1121.
- [12] Stuart Hadfield et al. “Quantum approximate optimization with hard and soft constraints”. In: *Proceedings of the Second International Workshop on Post Moores Era Supercomputing*. 2017, pp. 15–21.
- [13] Tadashi Kadowaki and Hidetoshi Nishimori. “Quantum annealing in the transverse Ising model”. In: *Physical Review E* 58.5 (Nov. 1998), 5355–5363. ISSN: 1095-3787. DOI: [10.1103/physreve.58.5355](https://doi.org/10.1103/physreve.58.5355). URL: <http://dx.doi.org/10.1103/PhysRevE.58.5355>.
- [14] Edward Farhi et al. “Quantum Computation by Adiabatic Evolution”. In: (2000). arXiv: [quant-ph/0001106](https://arxiv.org/abs/quant-ph/0001106) [quant-ph]. URL: <https://arxiv.org/abs/quant-ph/0001106>.
- [15] Satoshi Morita and Hidetoshi Nishimori. “Mathematical foundation of quantum annealing”. In: *Journal of Mathematical Physics* 49.12 (2008).
- [16] Atanu Rajak et al. “Quantum annealing: An overview”. In: *Philosophical Transactions of the Royal Society A* 381.2241 (2023), p. 20210417.
- [17] Alberto Peruzzo et al. “A variational eigenvalue solver on a photonic quantum processor”. In: *Nature Communications* 5.1 (July 2014). ISSN: 2041-1723. DOI: [10.1038/ncomms5213](https://doi.org/10.1038/ncomms5213). URL: <http://dx.doi.org/10.1038/ncomms5213>.
- [18] Jarrod R McClean et al. “The theory of variational hybrid quantum-classical algorithms”. In: *New Journal of Physics* 18.2 (Feb. 2016), p. 023023. ISSN: 1367-2630. DOI: [10.1088/1367-2630/18/2/023023](https://doi.org/10.1088/1367-2630/18/2/023023). URL: <http://dx.doi.org/10.1088/1367-2630/18/2/023023>.
- [19] A. Yu. Kitaev. “Quantum measurements and the Abelian Stabilizer Problem”. In: (1995). arXiv: [quant-ph/9511026](https://arxiv.org/abs/quant-ph/9511026) [quant-ph]. URL: <https://arxiv.org/abs/quant-ph/9511026>.
- [20] Guido Pagano et al. “Quantum approximate optimization of the long-range Ising model with a trapped-ion quantum simulator”. In: *Proceedings of the National Academy of Sciences* 117.41 (Oct. 2020), 25396–25401. ISSN: 1091-6490. DOI: [10.1073/pnas.2006373117](https://doi.org/10.1073/pnas.2006373117). URL: <http://dx.doi.org/10.1073/pnas.2006373117>.
- [21] G. E. L. Peixe et al. “Using a Feedback-Based Quantum Algorithm to Analyze the Critical Properties of the ANNNI Model Without Classical Optimization”. In: (2024). arXiv: [2406.17937](https://arxiv.org/abs/2406.17937) [quant-ph]. URL: <https://arxiv.org/abs/2406.17937>.
- [22] Alicia B. Magann et al. “Feedback-Based Quantum Optimization”. In: *Physical Review Letters* 129.25 (Dec. 2022). ISSN: 1079-7114. DOI: [10.1103/physrevlett.129.250502](https://doi.org/10.1103/physrevlett.129.250502). URL: <http://dx.doi.org/10.1103/PhysRevLett.129.250502>.
- [23] Phillip C. Lotshaw et al. “Simulations of frustrated Ising Hamiltonians using quantum approximate optimization”. In: *Philosophical Transactions of the Royal*

- Society A: Mathematical, Physical and Engineering Sciences* 381.2241 (Dec. 2022). ISSN: 1471-2962. DOI: [10.1098/rsta.2021.0414](https://doi.org/10.1098/rsta.2021.0414). URL: <http://dx.doi.org/10.1098/rsta.2021.0414>.
- [24] Stefan H. Sack and Maksym Serbyn. “Quantum annealing initialization of the quantum approximate optimization algorithm”. In: *Quantum* 5 (July 2021), p. 491. ISSN: 2521-327X. DOI: [10.22331/q-2021-07-01-491](https://doi.org/10.22331/q-2021-07-01-491). URL: <http://dx.doi.org/10.22331/q-2021-07-01-491>.
- [25] Mark W Johnson et al. “Quantum annealing with manufactured spins”. In: *Nature* 473.7346 (May 2011), pp. 194–198. DOI: [10.1038/nature10012](https://doi.org/10.1038/nature10012). URL: <https://doi.org/10.1038/nature10012>.
- [26] P. I. Bunyk et al. “Architectural Considerations in the Design of a Superconducting Quantum Annealing Processor”. In: *IEEE Transactions on Applied Superconductivity* 24.4 (Aug. 2014), 1–10. ISSN: 1558-2515. DOI: [10.1109/tasc.2014.2318294](https://doi.org/10.1109/tasc.2014.2318294). URL: <http://dx.doi.org/10.1109/TASC.2014.2318294>.
- [27] Andrew D. King et al. “Observation of topological phenomena in a programmable lattice of 1,800 qubits”. In: *Nature* 560.7719 (Aug. 2018), 456–460. ISSN: 1476-4687. DOI: [10.1038/s41586-018-0410-x](https://doi.org/10.1038/s41586-018-0410-x). URL: <http://dx.doi.org/10.1038/s41586-018-0410-x>.
- [28] Andrew D. King et al. “Quantum Annealing Simulation of Out-of-Equilibrium Magnetization in a Spin-Chain Compound”. In: *PRX Quantum* 2 (3 2021), p. 030317. DOI: [10.1103/PRXQuantum.2.030317](https://doi.org/10.1103/PRXQuantum.2.030317). URL: <https://link.aps.org/doi/10.1103/PRXQuantum.2.030317>.
- [29] Elijah Pelofske, Andreas Bärttschi, and Stephan Eidenbenz. “Simulating Heavy-Hex Transverse Field Ising Model Magnetization Dynamics Using Programmable Quantum Annealers”. In: (2024). arXiv: [2311.01657](https://arxiv.org/abs/2311.01657) [quant-ph]. URL: <https://arxiv.org/abs/2311.01657>.
- [30] Sepehr Ebadi et al. “Quantum phases of matter on a 256-atom programmable quantum simulator”. In: *Nature* 595.7866 (July 2021), 227–232. ISSN: 1476-4687. DOI: [10.1038/s41586-021-03582-4](https://doi.org/10.1038/s41586-021-03582-4). URL: <http://dx.doi.org/10.1038/s41586-021-03582-4>.
- [31] G. Semeghini et al. “Probing topological spin liquids on a programmable quantum simulator”. In: *Science* 374.6572 (Dec. 2021), 1242–1247. ISSN: 1095-9203. DOI: [10.1126/science.abi8794](https://doi.org/10.1126/science.abi8794). URL: <http://dx.doi.org/10.1126/science.abi8794>.
- [32] Dolev Bluvstein et al. “A quantum processor based on coherent transport of entangled atom arrays”. In: *Nature* 604.7906 (Apr. 2022), 451–456. ISSN: 1476-4687. DOI: [10.1038/s41586-022-04592-6](https://doi.org/10.1038/s41586-022-04592-6). URL: <http://dx.doi.org/10.1038/s41586-022-04592-6>.
- [33] Andrew D King et al. “Quantum critical dynamics in a 5,000-qubit programmable spin glass”. In: *Nature* 617.7959 (2023), pp. 61–66.
- [34] J Oitmaa. “Frustrated transverse-field Ising model”. In: *Journal of Physics A: Mathematical and Theoretical* 53.8 (2020), p. 085001. DOI: [10.1088/1751-8121/ab63e6](https://doi.org/10.1088/1751-8121/ab63e6). URL: <https://dx.doi.org/10.1088/1751-8121/ab63e6>.
- [35] N. Kellermann, M. Schmidt, and F. M. Zimmer. “Quantum Ising model on the frustrated square lattice”. In: *Phys. Rev. E* 99 (1 2019), p. 012134. DOI: [10.1103/PhysRevE.99.012134](https://doi.org/10.1103/PhysRevE.99.012134). URL: <https://link.aps.org/doi/10.1103/PhysRevE.99.012134>.
- [36] A. Bobák et al. “Frustrated spin- $\frac{1}{2}$  Ising antiferromagnet on a square lattice in a transverse field”. In: *Phys. Rev. E* 97 (2 2018), p. 022124. DOI: [10.1103/PhysRevE.97.022124](https://doi.org/10.1103/PhysRevE.97.022124). URL: <https://link.aps.org/doi/10.1103/PhysRevE.97.022124>.
- [37] A K Murtazaev, M K Ramazanov, and F A Kassan-Ogly. “Frustrations and phase transitions in the Ising model on square lattice”. In: *Journal of Physics: Conference Series* 510.1 (2014), p. 012026. DOI: [10.1088/1742-6596/510/1/012026](https://doi.org/10.1088/1742-6596/510/1/012026). URL: <https://dx.doi.org/10.1088/1742-6596/510/1/012026>.
- [38] Zhenyue Zhu and Steven R. White. “Quantum phases of the frustrated XY models on the honeycomb lattice”. In: *Modern Physics Letters B* 28.31 (2014), p. 1430016. DOI: [10.1142/S0217984914300166](https://doi.org/10.1142/S0217984914300166). eprint: <https://doi.org/10.1142/S0217984914300166>. URL: <https://doi.org/10.1142/S0217984914300166>.
- [39] Jeff Bezanson et al. “Julia: A fresh approach to numerical computing”. In: *SIAM review* 59.1 (2017), pp. 65–98. URL: <https://doi.org/10.1137/141000671>.
- [40] John Golden et al. “JuliQAOA: Fast, Flexible QAOA Simulation”. In: *Proceedings of the SC '23 Workshops of The International Conference on High Performance Computing, Network, Storage, and Analysis*. SC-W 2023. ACM, Nov. 2023. DOI: [10.1145/3624062.3624220](https://doi.org/10.1145/3624062.3624220). URL: <http://dx.doi.org/10.1145/3624062.3624220>.
- [41] E. Anderson et al. *LAPACK Users' Guide*. Third. Philadelphia, PA: Society for Industrial and Applied Mathematics, 1999. ISBN: 0-89871-447-8 (paperback).
- [42] Roger Fletcher. *Practical methods of optimization*. John Wiley & Sons, 2000.
- [43] Elizabeth Crosson et al. “Different strategies for optimization using the quantum adiabatic algorithm”. In: *arXiv preprint arXiv:1401.7320* (2014).
- [44] Xinwei Lee et al. “A depth-progressive initialization strategy for quantum approximate optimization algorithm”. In: *Mathematics* 11.9 (2023), p. 2176.
- [45] John Preskill. “Quantum Computing in the NISQ era and beyond”. In: *Quantum* 2 (Aug. 2018), p. 79. ISSN: 2521-327X. DOI: [10.22331/q-2018-08-06-79](https://doi.org/10.22331/q-2018-08-06-79). URL: <http://dx.doi.org/10.22331/q-2018-08-06-79>.
- [46] Alexey Galda et al. “Transferability of optimal QAOA parameters between random graphs”. In: *2021 IEEE International Conference on Quantum Computing and Engineering (QCE)*. IEEE, 2021, pp. 171–180.
- [47] Ruslan Shaydulin et al. “Parameter transfer for quantum approximate optimization of weighted maxcut”. In:

*ACM Transactions on Quantum Computing* 4.3 (2023), pp. 1–15.

- [48] Jahan Claes and Wim van Dam. “Instance Independence of Single Layer Quantum Approximate Optimization Algorithm on Mixed-Spin Models at Infinite Size”. In: *Quantum* 5 (Sept. 2021), p. 542. ISSN: 2521-327X. DOI: [10.22331/q-2021-09-15-542](https://doi.org/10.22331/q-2021-09-15-542). URL: <https://doi.org/10.22331/q-2021-09-15-542>.
- [49] Jonathan Wurtz and Danylo Lykov. “The fixed angle conjecture for QAOA on regular MaxCut graphs”. In: (2021). arXiv: [2107.00677](https://arxiv.org/abs/2107.00677) [quant-ph]. URL: <https://arxiv.org/abs/2107.00677>.
- [50] A Yu Chernyavskiy and BI Bantysh. “A Method to Compute QAOA Fixed Angles”. In: *Russian Microelectronics* 52.Suppl 1 (2023), S352–S356.
- [51] Sami Boulebnane and Ashley Montanaro. “Predicting parameters for the Quantum Approximate Optimization Algorithm for MAX-CUT from the infinite-size limit”. In: (2021). arXiv: [2110.10685](https://arxiv.org/abs/2110.10685) [quant-ph]. URL: <https://arxiv.org/abs/2110.10685>.
- [52] V. Akshay et al. “Parameter concentrations in quantum approximate optimization”. In: *Physical Review A* 104.1 (July 2021). ISSN: 2469-9934. DOI: [10.1103/physreva.104.L010401](https://doi.org/10.1103/physreva.104.L010401). URL: <http://dx.doi.org/10.1103/PhysRevA.104.L010401>.